Journal of Materials Chemistry

Cite this: J. Mater. Chem., 2012, 22, 15255

www.rsc.org/materials

PAPER

Probing the pore structure of a chiral periodic mesoporous organosilica using liquid crystals†

Vallamkondu Jayalakshmi,[a] Thomas Wood,[a] Rajratan Basu,[b] Jenny Du,[a] Thomas Blackburn,[a] Charles Rosenblatt,[b] Cathleen M. Crudden*[a] and Robert P. Lemieux*[a]

Received 15th May 2012, Accepted 21st June 2012
DOI: 10.1039/c2jm33089j

Periodic mesoporous organosilicas (PMO) are prepared by the surfactant-templated condensation of bridged organosilsesquioxane monomers. By controlling the nature of the organic segment, the type of surfactant and the condensation conditions, one can control the physical and chemical properties of the resulting PMO and produce highly ordered porous structures with a periodicity on the nanometer scale. The development of chiral PMO materials has been of significant interest given their potential in heterogeneous asymmetric catalysis, chiral chromatography and non-linear optics. Characterization of the chirality of pore structures in these materials thus far has been achieved by indirect methods including polarimetry and solid-state circular dichroism. We report herein a general and convenient approach to probe directly the pore structure of chiral PMO materials based on their interactions with inexpensive liquid crystalline solvents, which result in the induction of measurable chiral properties in the nematic (N) and smectic A (SmA) phases of the liquid crystals. The templated co-condensation of a biphenylene organosilsesquioxane monomer and a chiral binaphthyl organosilsesquioxane monomer produced a new chiral PMO material that was investigated as dopant in two different liquid crystal hosts. Measurements of induced circular dichroism and helical pitch in the nematic phase of the cyanobiphenyl liquid crystal **5CB**, and the measurement of an induced electroclinic effect in the SmA phase of the phenyl benzoate liquid crystal **9OO4** were carried out. The induced chiral properties measured in these experiments are consistent with chirality transfer taking place inside the pores, and suggest that the inner structure of the pores in the PMO material is indeed chiral.

Introduction

Periodic mesoporous organosilicas (PMO) have attracted significant attention in many communities since they were first reported by the groups of Stein, Ozin and Inagaki more than a decade ago.[1] These materials are prepared by the surfactant-templated condensation of bridged organosilsesquioxane monomers, *e.g.*, $(EtO)_3Si–R–Si(OEt)_3$ (Fig. 1). The surfactant serves to introduce porosity and order into the resulting organic–inorganic composites while the bridging organic segments (R) impart functionality and reactivity to the materials.[1] By controlling the nature of the organic segment, the type of surfactant and the condensation conditions, one can control the physical and chemical properties of the resulting PMO materials and produce highly ordered porous structures with a periodicity on the nanometer scale. The preparation of PMO materials constitutes a unique bottom-up approach to the development of functional materials that have found numerous applications in catalysis, chromatography and host–guest chemistry.[2]

The incorporation of organic segments within the walls of PMO materials also provides the opportunity to create materials with macroscopic chirality by using chiral organosilsesquioxane monomers.[3] Hence, the development of chiral PMO materials has been of significant interest given their potential impact in heterogeneous asymmetric catalysis, chiral chromatography and non-linear optics. Early examples of chiral PMO syntheses in which the chiral structure is incorporated into the PMO backbone required the addition of large quantities of silica precursor such as $Si(OEt)_4$ (TEOS) in addition to the chiral organosilsesquioxane monomer in order to obtain materials with any degree of order or porosity.[4–8] More recently, efforts have focused on the templated co-condensation of chiral and achiral organosilsesquioxane monomers,[3,9–11] or the self-condensation of purely chiral organosilsesquioxane monomers in order to obtain chiral PMO materials with a higher chiral content than that normally achieved with TEOS-based chiral PMOs.[12–17]

[a]Chemistry Department, Queen's University, Kingston, Ontario, Canada. E-mail: lemieux@chem.queensu.ca
[b]Department of Physics, Case Western Reserve University, Cleveland, Ohio 44106-7079, USA

† Electronic supplementary information (ESI) available: Synthetic procedures, N_2 adsorption/desorption isotherms, CP-MAS ^{29}Si and ^{13}C NMR spectra of PMO materials and UV spectrum of **5CB**. See DOI: 10.1039/c2jm33089j

Fig. 1 Surfactant-templated condensation of bridged organosilsesquioxane monomers.

We recently designed chiral PMOs based on a new chiral amplification strategy in which two complementary organosilsesquioxane monomers are co-condensed: one is a chiral monomer acting as a 'dopant' and the other is an achiral 'bulk' monomer with a structure that enables an efficient transfer of chirality from the dopant through the bulk of the PMO.[3,9] Atropisomeric biaryls such as **3–5** are the preferred chiral monomers for these PMO materials since they do not racemize under acidic or basic conditions, nor do they undergo thermal racemization at temperatures as high as 200 °C. Most importantly, they can effectively transfer their chirality *via* conformational interactions with achiral biphenylene monomers such as **2**.[18] Using this approach, chiral PMO materials with high organic content and relatively small proportions of valuable chiral monomer can be obtained. For example, PMO materials prepared by co-condensation of the bulk monomer **2** and the chiral monomer **3** (Chart 1) show evidence of chirality transfer in the bulk based on solid state CD spectroscopy, and co-condensation of the bulk monomer **1** and chiral monomer **4** (Chart 1) produces PMO fibers with a helical morphology that becomes more pronounced with increasing proportion of **4**.[3,9] Using the chiral monomer **5** both as a dopant and a ligating site for transition metals, we recently prepared PMO materials that are highly enantioselective hydrogenation catalysts.[19]

There are only a few reports in the literature on the characterization of chiral structures in PMO materials, and in most cases these have been limited to measurements of optical rotation or circular dichroism of chiral PMO materials as powders suspended in a liquid or KBr pellet,[4–6,9,15] or as thin films prepared by spin coating.[13,16] However, none of these approaches provides direct information on the chirality of the *pore structure*; at best, they provide indirect information about the chirality of the bulk material. Others have sought to establish the enantiomeric purity of the chiral monomer in PMO structures by decomposition of the silica network and analysis of the chiral residue by polarimetry,[8,17] circular dichroism spectroscopy,[10] or chiral phase HPLC.[14] The only example of a direct probe of chiral pore structure was reported by Kuschel *et al.* who showed that the (*R*)- and (*S*)-enantiomers of the chiral gas propylene oxide were differentially adsorbed by a chiral PMO material.[13] In this paper, we report a more general and convenient approach to probe the pore structure of chiral PMO materials based on their interactions with inexpensive liquid crystalline solvents, which result in the induction of measurable chiral properties in the nematic (N) and smectic A (SmA) phases of the liquid crystals. Furthermore, by using materials with blocked pores in control experiments, we are able to relate these effects directly to the pore structure of the materials.

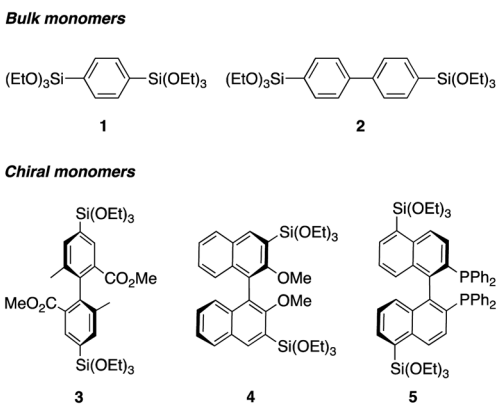

Chart 1 Bulk and chiral organosilsesquioxane monomers.

The effect of a chiral guest (dopant) on the properties of a liquid crystal host depends on molecular recognition to process and propagate the chiral perturbation exerted by the dopant on the host molecules.[18,20] In a nematic phase, which is characterized by orientational order of molecular long axes along a director $\hat{n}$, the chiral perturbation induced by the addition of a dopant results in a macroscopic helical structure with a pitch p that is inversely proportional to the mole fraction of the dopant (Fig. 2). The helical twisting power of a chiral dopant depends on the twist elasticity of the liquid crystal and on the structural complementarity between dopant and nematic host to achieve chirality transfer.[18] However, chiral induction in a nematic phase is not limited to molecular dopants forming homogeneous mixtures with a liquid crystal host; chiral supramolecular structures including chiral surfaces, carbon nanotubes and functionalized gold nanoclusters have all been shown to induce a helical pitch in nematic liquid crystals.[21–23]

The SmA phase can also be a very sensitive chirality detector by virtue of the electroclinic effect induced by a chiral dopant.[24,25] The achiral SmA phase is characterized by a diffuse layer structure in which the director $\hat{n}$ is oriented perpendicular to the layer plane, and cannot be distinguished mechanically from the

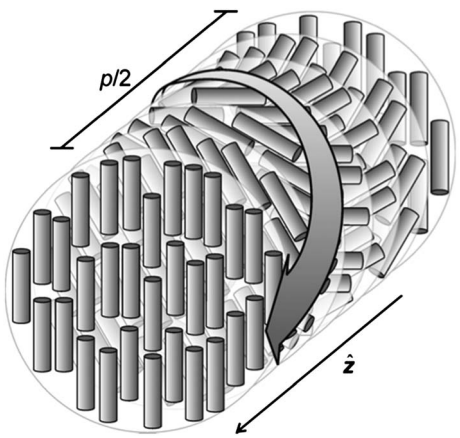

Fig. 2 Schematic representation of the chiral nematic phase. The director orientation rotates continuously along the *z*-axis.

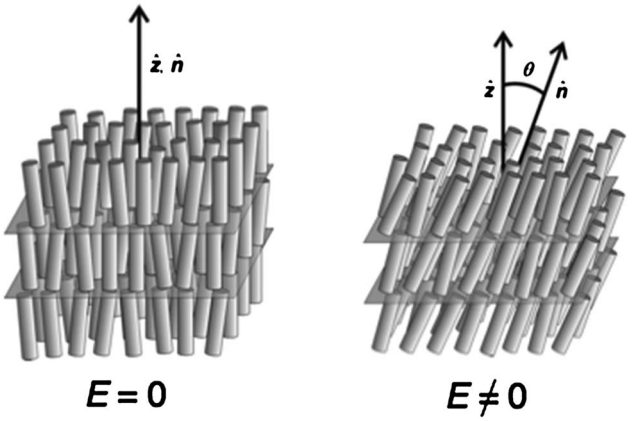

Fig. 3 Schematic representation of the electroclinic effect in the chiral SmA* phase. In this scheme, the electric field E is perpendicular to the plane of the page.

chiral SmA* phase in the absence of external perturbations. Garoff and Meyer have shown that an electric field E applied parallel to the layers of a chiral SmA* phase induces a molecular tilt θ relative to the layer normal $\hat{z}$ in a direction orthogonal to the field (Fig. 3).[26] This electroclinic effect is described by a phenomenological model derived from Landau theory that predicts a linear dependence of the induced tilt angle θ on the applied field E at low field strengths according to eqn (1), where e_c is the electroclinic coefficient.[27] Although generally observed in homogeneous liquid crystal formulations, an electroclinic effect was recently reported in a SmA liquid crystal doped with multiwall carbon nanotubes.[28]

$$\theta = e_c E \quad (1)$$

Hence, because of their fluid character and propensity to amplify the chirality of molecular and macromolecular dopants by induction of measurable chiral properties, the N and SmA phases of liquid crystal hosts can provide a unique and relatively simple means of probing the chirality of pore structures in PMO materials. We report herein the synthesis of a new chiral PMO material derived from the templated co-condensation of the biphenylene bulk monomer **2** and the chiral binaphthyl monomer **4**, and the direct probing of its chiral pore structure by measurements of induced chiral properties in two liquid crystal hosts. These include the measurements of induced circular dichroism and helical pitch in the nematic phase of the cyanobiphenyl liquid crystal **5CB**, and the measurement of an induced electroclinic effect in the SmA phase of the phenyl benzoate liquid crystal **9OO4**.

Results and discussion

PMO synthesis

The chiral binaphthyl monomer **4** was prepared according to our published procedure,[3] and co-condensed with the bulk monomer 4,4′-bis-(triethoxysilyl)biphenyl (**2**) to prepare the chiral PMO materials. A variety of surfactants and reaction conditions were tested for the templated co-condensation using a mixture of **2** and racemic (*rac*)-**4** in an 85 : 15 (w/w) ratio, which are summarized in Table 1 (see ESI† for Experimental details). The nonionic, alkylpolyether surfactant Brij 76 gave the best results, yielding a well ordered mesoporous material (*rac*)-**15-QPMO1-*ex*** after extraction of the surfactant with acidic ethanol. Analysis of this material by ^{13}C CP-MAS NMR confirmed the incorporation of the chiral binaphthyl monomer into the PMO structure (ESI,† Fig. 3), and the ^{29}Si CP-MAS NMR spectrum showed only peaks corresponding to T-sites (Fig. 5c), which indicates that no cleavage of Si–C bonds had occurred. Powder X-ray diffraction shows an intense peak corresponding to a *d*-spacing of 67 Å (ESI,† Fig. 4), and TEM imaging shows a structure with 2D hexagonal mesostructural order and an estimated lattice constant of 60 Å that is consistent with the XRD data (Fig. 5a and b). Interestingly, no incorporation of the chiral monomer was detected when the co-condensation was carried out under basic conditions using cetyltrimethylammonium bromide (CTAB) as surfactant, although this is consistent with our previous results.[9] Co-condensation with the Pluronic surfactant P123 under acidic conditions gave a poorly ordered microporous

Table 1 Surfactants and conditions screened for the co-condensation of monomers **2** and (*rac*)-**4** in an 85 : 15 (w/w) ratio to give (*rac*)-**15-QPMO1-*ex***

Surfactant/catalyst	Condensation conditions	Aging conditions
Brij 76/HCl	60 °C, 20 h	80 °C, 24 h
CTAB/NaOH	rt, 20 h	95 °C, 20 h
P123/HCl	40 °C, 24 h	95 °C, 20 h
F127/HCl	40 °C, 24 h	100 °C, 24 h

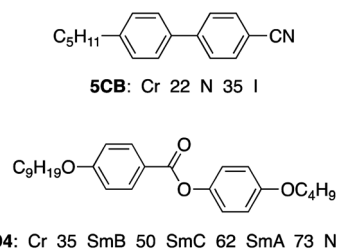

Fig. 4 Achiral liquid crystal hosts and phase transition temperatures.

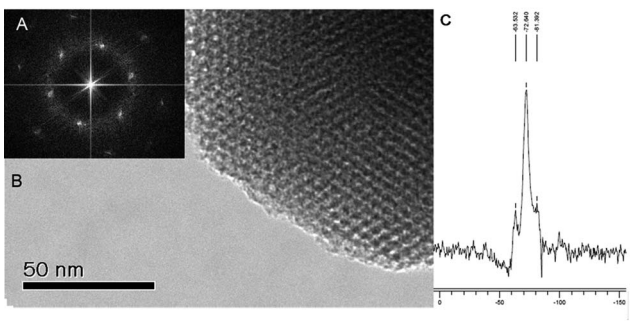

Fig. 5 (a) FFT and (b) TEM images showing the 2D hexagonally ordered mesostructure of (*rac*)-**15-QPMO1-*ex*** synthesized using Brij 76 as surfactant; (c) ^{29}Si CP-MAS NMR spectrum of (*rac*)-**15-QPMO1-*ex*** showing the presence of T-sites only in the PMO.

Table 2 Physicochemical properties derived from N_2 adsorption/desorption isotherms for chiral PMO materials obtained by templated co-condensation of **2** and either (*R*)- or (*S*)-**4** using Brij 76 under acidic conditions after surfactant extraction

PMO[a]	**2** : **4** (w/w)	BET surface area ($m^2\ g^{-1}$)	Avg. pore diameter (nm)[b]	Avg. pore volume ($cm^3\ g^{-1}$)[b]
(*R*)-**5-QPMO1-*ex***	95 : 5	878	2.79	0.71
(*S*)-**5-QPMO1-*ex***	95 : 5	957	2.86	0.76
(*R*)-**15-QPMO1-*ex***	85 : 15	871	2.28	0.60
(*S*)-**15-QPMO1-*ex***	85 : 15	838	2.26	0.56
(*R*)-**30-QPMO1-*ex***	70 : 30	818	1.94	0.45
(*S*)-**30-QPMO1-*ex***	70 : 30	926	2.06	0.55
(*S*)-**100-QPMO1-*ex***	0 : 100	432	1.26	0.25

[a] The suffix '*ex*' refers to the pores being free of surfactant after extraction with acidic ethanol. [b] Values taken from the BJH adsorption branch.

material according to nitrogen physisorption analysis, whereas co-condensation with the related surfactant F127 under similar conditions produced very little bulk material.

Using the optimized conditions with Brij 76 as surfactant, PMOs were synthesized using optically pure (*R*)- or (*S*)-**4** in varying ratios (w/w) with the bulk monomer **2**. Following each co-condensation reaction, the templating surfactant was removed by Soxhlet extraction in acidic ethanol. The physicochemical properties of the resulting PMO materials were derived from their N_2 adsorption/desorption isotherms (Table 2) and suggest that increasing the weight fraction of chiral monomer in the PMO materials causes a decrease in average pore diameter and pore volume. These results are consistent with previous observations that condensation of monomers with more bulk and/or functionality leads to PMO materials of poorer quality,[3,9] and validate the use of a co-condensation strategy based on chiral amplification to produce high quality chiral PMO materials.

Given the consistency in average pore diameter and pore volume measurements for (*R*)- and (*S*)-**15-QPMO1-*ex***, and the appropriate balance between chiral content and pore diameter, these two materials were chosen for further investigation as dopants in liquid crystal hosts. To allow for appropriate control experiments (*vide infra*), the chiral PMO materials were isolated in two different states: (i) with the surfactant still present in the pores (*i.e.*, with the pores blocked, **15-QPMO1-*as***), and (ii) after removal of the surfactant by Soxhlet extraction with acidic ethanol (*i.e.*, with the pores free of surfactant, **15-QPMO1-*ex***). The use of the surfactant as a 'plug' for the pores of templated mesostructured materials is not without precedent, but has been optimized by our group.[29,30]

Helical pitch measurements

A 1% (w/w) mixture of the chiral PMO material with surfactant-free pores (*S*)-**15-QPMO1-*ex*** in the achiral liquid crystal 4-cyano-4′-pentylbiphenyl (**5CB**) was first analyzed by polarized optical microscopy (POM) as a film between an untreated glass slide and cover slip. The analysis revealed a Schlieren texture characteristic of an achiral N phase (Fig. 6). A chiral nematic (N*) phase with a helical pitch on the order of the film thickness

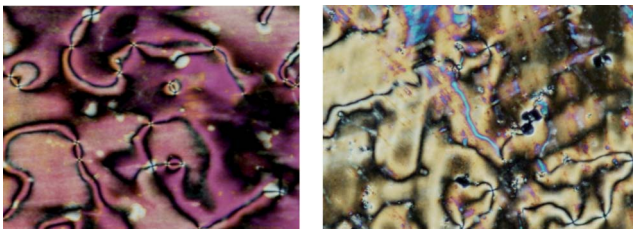

Fig. 6 Polarized micrographs of unaligned films of (a) **5CB** at 25 °C (left) and (b) a 1% (w/w) mixture of (*S*)-**15-QPMO1-*ex*** in **5CB** at 25 °C (right). The difference in interference colors is due to a variation in film thickness.

normally exhibits a fingerprint or Grandjean texture;[31] the absence of such textures in this case could be taken as evidence ruling out chiral induction, but it could also suggest that the induced pitch is significantly greater than the film thickness, perhaps >100 μm. To determine if a helical pitch of that length scale was formed, we measured the curvature of reverse twist disclination lines formed by the 1% (*S*)-**15-QPMO1-*ex*/5CB** mixture in a 90° twisted nematic (TN) cell according to the method of Raynes.[32]

In the absence of an inherent N* pitch, domains with right- and left-handed twists are energetically equivalent in a 90° TN cell, thus resulting in linear disclination lines that terminate at the cell spacers (Fig. 7a). However, for a N* liquid crystal with a helical pitch p of one handedness, domains with the same handedness of surface-imposed twist grow at the expense of those with opposite handedness, which results in bowed disclination lines with a radius of curvature R that is proportional to the pitch p according to eqn (2). A polarized micrograph of the 1% (*S*)-**15-QPMO1-*ex*/5CB** mixture in a 90° TN cell clearly shows bowed disclination lines with radii of curvature giving an average helical pitch of 1.3 ± 0.2 mm (Fig. 7b), which is orders of magnitude greater than the thickness of the film used in the initial texture analysis by POM and hence explains the absence of a Grandjean or fingerprint texture.

$$R = p/2 \tag{2}$$

On the other hand, when the chiral PMO with blocked pores (*S*)-**15-QPMO1-*as*** was analyzed by the same method as a 1% (w/w) mixture in **5CB**, significantly different results were obtained. As shown in the resulting micrograph (Fig. 7c), the disclination lines show no measurable curvature, which suggests that there is very little or no chiral induction when the pores are blocked, and that the chiral induction observed with (*S*)-**15-QPMO1-*ex*** does not result from interactions of the host **5CB**

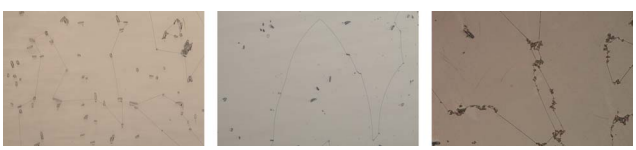

Fig. 7 Polarized micrographs of 90° twist cells at room temperature containing (a) **5CB**, (b) a 1% (w/w) mixture of (*S*)-**15-QPMO1-*ex*** in **5CB**, and (c) a 1% (w/w) mixture of (*S*)-**15-QPMO1-*as*** in **5CB**. The dark spots correspond to 10 μm spacers.

with the outer surfaces of the PMO particles but instead from interactions with the inner pore structures.

Circular dichroism spectroscopy

Aligned films of the 1% **15-QPMO1/5CB** mixtures were also analyzed by circular dichroism spectroscopy using an OLIS DSM 20 double beam instrument. For these measurements, the PMO-doped liquid crystal samples were sandwiched between polyvinyl alcohol (PVA)-coated quartz glass slides separated by Mylar spacers to give a film thickness of 6 ± 1 μm. The PVA-coated surfaces were rubbed in parallel directions with a cotton cloth to produce a uniform planar alignment of the **5CB** molecules, which was confirmed by polarized optical microscopy. The aligned films were mounted vertically on a rotating stage in the chamber of the CD spectrometer, with the rubbing direction coincident with the axis of the linear polarizer and rotated through successive 45° increments about an axis parallel to the incident beam. For each film, eight spectra were acquired at room temperature over a 360° rotation; the eight spectra were averaged in order to remove linear dichroism and birefringence artifacts,[23,33] which are usually observed with anisotropic samples when the circularly polarized incident beam is generated by a photoelastic modulator.[34]

The liquid crystal host **5CB** is characterized by a UV absorbance maximum at 280 nm (Fig. 15 in ESI†), and a film of neat **5CB** with a thickness of 6 μm results in a saturation of the absorbance up to *ca.* 315 nm. As shown in Fig. 8, the CD spectrum of a 1% (w/w) mixture of (*R*)-**15-QPMO1-*ex*** in **5CB** shows a positive band beyond the absorbance cutoff, with a maximum at 325 nm. This CD spectrum is consistent with that previously reported by Wu *et al.* for a liquid crystalline acrylate copolymer containing cyanobiphenyl and photochromic azobenzene side-chains in a ratio of 85 : 15 after irradiation with circularly polarized light.[35] The spectrum reported by Wu *et al.* was acquired with a thinner sub-micron film of the copolymer

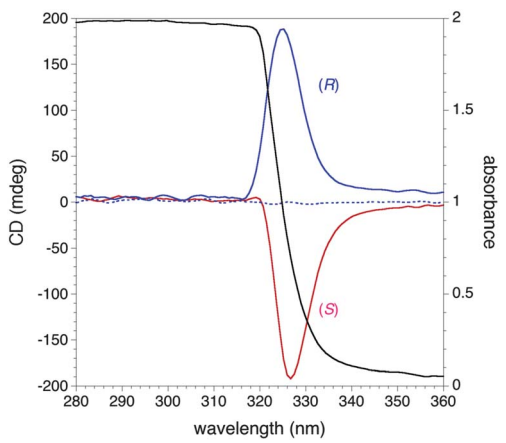

Fig. 8 CD spectra of 1% (w/w) mixtures of (*R*)-**15-QPMO1-*ex*** in **5CB** (blue line), (*S*)-**15-QPMO1-*ex*** in **5CB** (red line) and (*R*)-**15-QPMO1-*as*** in **5CB** (dashed blue line) as 6 μm films at room temperature.[36] Each spectrum is the average of eight scans taken every 45° over a 360° rotation about an axis parallel to the incident light beam. The UV absorption spectrum of a 6 μm film of **5CB** is also shown (black line) indicating the absorption cutoff due to the high optical density of the **5CB** film.

produced by spin coating and featured bands of opposite signs at 265 and 325 nm with a crossover point at 280 nm, which is characteristic of a split Cotton effect produced by cyanobiphenyl chromophores organized in a helical structure. In the spectrum shown in Fig. 8, the opposite CD band of the split Cotton effect cannot be observed because of the absorption cutoff at 315 nm. The CD spectrum of the 1% (*S*)-**15-QPMO1-*ex*/5CB** mixture is a mirror image of that obtained with the 1% (*R*)-**15-QPMO1-*ex*/5CB** mixture, which confirms the expected enantiomeric relationship of the two materials.[36]

On the other hand, the CD spectrum of a 1% mixture of the PMO with blocked pores (*S*)-**15-QPMO1-*as*** in **5CB** does not show any CD band above the 315 nm cutoff, nor does the CD spectrum of either the (*R*)- or (*S*)-**15-QPMO1-*ex*/5CB** mixture when the sample is heated above 35 °C, the transition temperature at which the nematic phase turns into an isotropic liquid phase (*i.e.*, the clearing point). These results, taken together with the helical pitch measurements, suggest that the CD band observed at room temperature with the surfactant-free chiral PMO dopant in **5CB** results from a chiral distortion of the N phase that propagates in the liquid crystal host, and support the conclusion that chiral induction in **5CB** originates from interactions of the liquid crystal molecules with the inner structure of the pores.

Electroclinic measurements

To further demonstrate the use of liquid crystals to probe the inner structure of chiral pores in PMO materials, we measured the induced electroclinic effect in the SmA phase of a liquid crystal doped with (*S*)-**15-QPMO1**. In this experiment, an electric field *E* is applied across aligned films of 1% (w/w) mixtures of (*S*)-**15-QPMO1**, either with blocked pores or surfactant-free pores, in the liquid crystal host 4-butyloxyphenyl 4-nonyloxybenzoate (**9OO4**), and the induced tilt angle θ is measured as a function of *E*. The two planar-aligned samples were prepared by spin-coating two pairs of conducting, semi-transparent indium-tin-oxide (ITO)-coated glass slides with the polyamic acid RN-1175 (Nissan Chemical Industries). Imidization was achieved by prebaking for 15 min at 80 °C and then for 50 min at 180 °C. The slides were then rubbed using a cotton cloth attached to a rolling drum, and cells of *ca.* 10 μm thickness were constructed and filled by capillary action with the (*S*)-**15-QPMO1/9OO4** mixtures. The optical setup used to measure the induced electroclinic effect is known as the 'classical electroclinic geometry',[37] and consists of a beam from a 5 mW He–Ne laser at 633 nm that passes through a polarizer, the cell, a crossed analyzer and into a detector. The beam is polarized at an angle of $\pi/8$ with respect to the rubbing direction of the cell. The output of the detector is fed into both a lock-in amplifier operating in amplitude-phase mode and referenced to the driving frequency of the applied electric field ($f = 1000$ Hz) and to a dc voltmeter, allowing us to measure the ac intensity I_{ac} at frequency f and the dc intensity I_{dc}, respectively. The field-induced spatially-averaged tilt angle θ is obtained from the measured intensities according to eqn (3):[37]

$$\theta = I_{ac}/4I_{dc} \quad (3)$$

In the case of the surfactant-free (*S*)-**15-QPMO1-*ex*/9OO4** mixture, an electroclinic effect is observed in the SmA phase. As

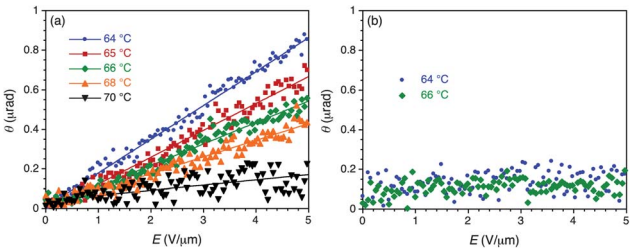

Fig. 9 Electroclinic effect measured as the spatially-averaged amplitude of the tilt angle θ *vs.* electric field E at different temperatures in the SmA phase of 1% (w/w) mixtures of (a) (*S*)-**15-QPMO1-*ex*** in **9OO4**, and (b) (*S*)-**15-QPMO1-*as*** in **9OO4**.

shown in Fig. 9a, the average director tilt angle θ is proportional to the applied field E, and the electroclinic coefficient e_c (eqn (1)) increases with decreasing temperature on approaching the SmA*–SmC* phase transition. This behavior is consistent with chiral induction in the liquid crystal host.[26] On the other hand, the pore-blocked (*S*)-**15-QPMO1-*as*/9OO4** mixture shows no apparent electroclinic effect at two different temperatures in the SmA phase (Fig. 9b),[38] which is consistent with the previous results and further supports the conclusion that the chiral induction observed in the two liquid crystal hosts originates from interactions of the liquid crystal molecules with the inner structure of the pores in the chiral PMO material.

Conclusions

Nematic and smectic A liquid crystal phases are anisotropic fluids that can diffuse into porous structures such as those of chiral PMO materials and report on the chiral topography of the inner structure of the pores based on the induction of detectable chiral properties in the liquid crystal material outside the pores. The facts that liquid crystal materials such as **5CB** and **9OO4** are relatively inexpensive, that the detection of chiral properties such as the helical pitch of the chiral N* phase and the electroclinic effect of the chiral SmA* phase are measurable by simple methods, and that very weak chiral perturbations may be detected by virtue of collective effects make this approach very attractive for the characterization of chiral PMO materials. In this study, we have shown that the chiral PMO **15-QPMO1** with pores free from the templating surfactant induces a measurable helical pitch in the liquid crystal host **5CB** and an electroclinic effect in the liquid crystal host **9OO4**, whereas the same chiral PMO with pores obstructed by the templating surfactant does not. These results are consistent with chirality transfer taking place inside the pores and propagating to the liquid crystal phase outside the pores, and therefore support the claim that the inner structure of the pores in **15-QPMO1** is indeed chiral. The application of these methods to other chiral PMO materials is currently underway in our laboratories and will be reported in due course.

Acknowledgements

This work was supported by the Natural Sciences and Engineering Research Council of Canada (Discovery, Accelerator and CREATE grants to C.M.C. and R.P.L.), and by the U.S. Department of Energy, Office of Basic Energy Sciences, Division of Materials Sciences and Engineering under Award DE-FG02-01ER45934 (R.B. and C.R.).

References

1 For reviews, see: N. Mizoshita, T. Tani and S. Inagaki, *Chem. Soc. Rev.*, 2011, **40**, 789; Q. Yang, J. Liu, L. Zhang and C. Li, *J. Mater. Chem.*, 2009, **19**, 1945; F. Hoffmann, M. Cornelius, J. Morell and M. Fröba, *Angew. Chem., Int. Ed.*, 2006, **45**, 3216; F. Hoffmann, M. Cornelius, J. Morell and M. Fröba, *J. Nanosci. Nanotechnol.*, 2006, **6**, 265; W. J. Hunks and G. A. Ozin, *J. Mater. Chem.*, 2005, **15**, 3716; B. Hatton, K. Landskron, W. Whitnall, D. Perovic and G. A. Ozin, *Acc. Chem. Res.*, 2005, **38**, 305.
2 For reviews, see: Q. Yang, J. Liu, L. Zhang and C. Li, *J. Mater. Chem.*, 2009, **19**, 1945; C. Li, H. Zhang, D. Jiang and Q. Yang, *Chem. Commun.*, 2007, **6**, 547; A. Corma and H. Garcia, *Adv. Synth. Catal.*, 2006, **348**, 1391; A. Walcarius, D. Mandler, J. A. Cox, M. Collinson and O. Lev, *J. Mater. Chem.*, 2005, **15**, 3663; A. Sayari, *Chem. Nanostruct. Mater.*, 2003, 39.
3 X. Wu, T. Blackburn, J. D. Webb, A. E. Garcia-Bennett and C. M. Crudden, *Angew. Chem., Int. Ed.*, 2011, **50**, 8095.
4 C. Baleizao, B. Gigante, D. Das, M. Alvaro, H. Garcia and A. Corma, *Chem. Commun.*, 2003, 1860.
5 M. Alvaro, M. Benitez, D. Das, B. Ferrer and H. Garcia, *Chem. Mater.*, 2004, **16**, 2222.
6 A. Ide, R. Voss, G. Scholz, G. Ozin, M. Antonietti and A. Thomas, *Chem. Mater.*, 2007, **19**, 2649.
7 R. A. Garcia, R. van Griecken, J. Iglesias, V. Morales and D. Gordillo, *Chem. Mater.*, 2008, **20**, 2964.
8 L. Zhang, J. Liu, J. Yang, Q. Yang and C. Li, *Chem.–Asian J.*, 2008, **3**, 1842.
9 S. MacQuarrie, M. Thompson, A. Blanc, N. Mosey, R. P. Lemieux and C. M. Crudden, *J. Am. Chem. Soc.*, 2008, **130**, 14099.
10 P. Wang, J. Yang, J. Liu, L. Zhang and Q. Yang, *Microporous Mesoporous Mater.*, 2009, **117**, 91.
11 R. A. Garcia, R. van Griecken, J. Iglesias, V. Morales and N. Villajos, *J. Catal.*, 2010, **274**, 221.
12 S. Polarz and A. Kuschel, *Adv. Mater.*, 2006, **18**, 1206.
13 A. Kuschel, H. Sievers and S. Polarz, *Angew. Chem., Int. Ed.*, 2008, **47**, 9513.
14 S. Inagaki, S. Y. Guan, Q. Yang, M. P. Kapoor and T. Shimada, *Chem. Commun.*, 2008, 202.
15 J. Morell, S. Chatterjee, P. J. Klar, D. Mauder, I. Shenderovich, F. Hoffmann and M. Fröba, *Chem.–Eur. J.*, 2008, **14**, 5935.
16 A. Kuschel and S. Polarz, *J. Am. Chem. Soc.*, 2010, **132**, 6558.
17 J. Y. Zhuang, J. Y. Shi, B. C. Ma and W. Wang, *J. Mater. Chem.*, 2010, **20**, 6026.
18 S. Pieraccini, S. Masiero, A. Ferrarini and G. P. Spada, *Chem. Soc. Rev.*, 2011, **40**, 258; S. Pieraccini, A. Ferrarini and G. P. Spada, *Chirality*, 2008, **20**, 749; G. P. Spada and G. Proni, *Enantiomer*, 1998, **3**, 301; G. Solladié and R. G. Zimmermann, *Angew. Chem.*, 1984, **96**, 335.
19 T. Seki, K. McEleney and C. M. Crudden, *Chem. Commun.*, 2012, **48**, 6369.
20 R. Eelkema and B. L. Feringa, *Org. Biomol. Chem.*, 2006, **4**, 3729; D. B. Amabilino and J. Veciana, *Top. Curr. Chem.*, 2006, **265**, 253.
21 Y. Choi, T. Atherton, S. Ferjani, R. G. Petschek and C. Rosenblatt, *Phys. Rev. E: Stat., Nonlinear, Soft Matter Phys.*, 2009, **80**, 060701; M. Nakata, G. Zanchetta, M. Buscaglia, T. Bellini and N. A. Clark, *Langmuir*, 2008, **24**, 10390; R. Berardi, H.-G. Kuball, R. Memmer and C. Zannoni, *J. Chem. Soc., Faraday Trans.*, 1998, **94**, 1229.
22 R. Basu, C.-L. Chen and C. Rosenblatt, *J. Appl. Phys.*, 2011, **109**, 083518.
23 H. Qi, J. O'Neil and T. Hegmann, *J. Mater. Chem.*, 2008, **18**, 374.
24 D. M. Walba, L. Eshdat, E. Korblova, R. Shao and N. A. Clark, *Angew. Chem., Int. Ed.*, 2007, **46**, 1473.
25 C. S. Hartley, N. Kapernaum, J. C. Roberts, F. Giesselmann and R. P. Lemieux, *J. Mater. Chem.*, 2006, **16**, 2329; T. Hegmann, M. R. Meadows, M. D. Wand and R. P. Lemieux, *J. Mater. Chem.*, 2004, **14**, 1; T. Hegmann and R. P. Lemieux, *J. Mater. Chem.*, 2002, **12**, 3368.

26 S. Garoff and R. B. Meyer, *Phys. Rev. Lett.*, 1977, **38**, 848.
27 I. Abdulhalim and G. Moddel, *Liq. Cryst.*, 1991, **9**, 493.
28 R. Basu, K. A. Boccuzzi, S. Ferjani and C. Rosenblatt, *Appl. Phys. Lett.*, 2010, **97**, 121908.
29 F. De Juan and E. Ruiz-Hitzky, *Adv. Mater.*, 2000, **12**, 430; A.-H. Lu, W.-C. Li, A. Kiefer, W. Schmidt, E. Bill, G. Fink and F. Schuth, *J. Am. Chem. Soc.*, 2004, **124**, 8616.
30 For other approaches, see: D. S. Shepard, W. Zhou, T. Maschmeyer, J. M. Matters, C. L. Roper, S. Parsons, B. F. G. Johnson and M. J. Duer, *Angew. Chem., Int. Ed.*, 1998, **37**, 2719; Y. Xie, S. Quinlivan and T. Asefa, *J. Phys. Chem. C*, 2008, **112**, 9996; N. Gartmann and D. Brühwiler, *Angew. Chem., Int. Ed.*, 2009, **48**, 6354; D. Brühwiler, *Nanoscale*, 2010, **2**, 4247.
31 I. Dierking, *Textures of Liquid Crystals*, Wiley-VCH, Weinheim, 2003.
32 E. P. Raynes, *Liq. Cryst.*, 2006, **33**, 1215.
33 C. Spitz, S. Dähne, A. Ouart and H.-W. Abraham, *J. Phys. Chem. B*, 2000, **104**, 8664; C. Nuckolls, T. J. Katz, T. Verbiest, S. Van Elshocht, H.-G. Kuball, S. Kiesewalter, A. J. Lovinger and A. Persoons, *J. Am. Chem. Soc.*, 1998, **120**, 8656; F. D. Saeva and G. R. Olin, *J. Am. Chem. Soc.*, 1976, **98**, 2709.
34 W. Kaminsky, K. Claborn and B. Kahr, *Chem. Soc. Rev.*, 2004, **33**, 514; J. Schellman and H. P. Jensen, *Chem. Rev.*, 1987, **87**, 1359; Y. Shindo and Y. Ohmi, *J. Am. Chem. Soc.*, 1985, **107**, 91; Å. Davidsson, B. Nordén and S. Seth, *Chem. Phys. Lett.*, 1980, **70**, 313.
35 Y. Wu, A. Natansohn and P. Rochon, *Macromolecules*, 2004, **37**, 6801.
36 The difference in λ_{ext} between the CD bands for the (*R*)- and (*S*)-**15-QPMO1-ex/5CB** mixtures is due to a small variation in film thickness and a corresponding shift in the absorption cutoff.
37 G. Andersson, I. Dahl, P. Keller, W. Kuczynski, S. T. Lagerwall, K. Skarp and B. Stebler, *Appl. Phys. Lett.*, 1987, **51**, 640.
38 The lock-in experiment was performed in amplitude/phase (R/θ) mode, and thus the observed signal is always positive, with the average signal corresponding to $\langle\theta^2\rangle^{1/2}$.